AD-A153 701 TWO-DEGREE-OF-FREEDOM LINEAR AND PLANAR MIRCOWAVE ARRAY LENSES(U) ROME AIR DEVELOPMENT CENTER GRIFFISS AFB NY D T MCGRATH OCT 84 RADC-TR-84-215 1/1

UNCLASSIFIED F/G 9/5 NL

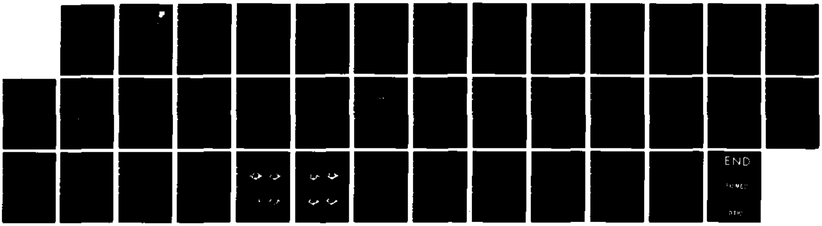

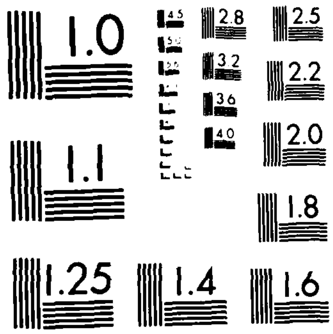

MICROCOPY RESOLUTION TEST CHART
NATIONAL BUREAU OF STANDARDS 1963-A

2

AD-A153 701

RADC-TR-84-215
In-House Report
October 1984

TWO-DEGREE-OF-FREEDOM LINEAR AND PLANAR MICROWAVE ARRAY LENSES

Daniel T. McGrath, Captain, USAF

ROME AIR DEVELOPMENT CENTER
Air Force Systems Command
Griffiss Air Force Base, NY 13441

This report has been reviewed by the RADC Public Affairs Office (PA) and is releasable to the National Technical Information Service (NTIS). At NTIS it will be releasable to the general public, including foreign nations.

RADC-TR-84-215 has been reviewed and is approved for publication.

APPROVED: John K. Schindler

JOHN K. SCHINDLER
Chief, Antennas & RF Components Branch
Electromagnetic Sciences Division

APPROVED: Allan C. Schell

ALLAN C. SCHELL
Chief, Electromagnetic Sciences Division

FOR THE COMMANDER: John A. Ritz

JOHN A. RITZ
Acting Chief, Plans Office

If your address has changed or if you wish to be removed from the RADC mailing list, or if the addressee is no longer employed by your organization, please notify RADC (EEAA) Hanscom AFB MA 01731. This will assist us in maintaining a current mailing list.

Do not return copies of this report unless contractual obligations or notices on a specific document requires that it be returned.

Unclassified

SECURITY CLASSIFICATION OF THIS PAGE

AD-A153701

REPORT DOCUMENTATION PAGE

1a. REPORT SECURITY CLASSIFICATION: Unclassified	1b. RESTRICTIVE MARKINGS
2a. SECURITY CLASSIFICATION AUTHORITY	3. DISTRIBUTION/AVAILABILITY OF REPORT: Approved for public release; distribution unlimited.
2b. DECLASSIFICATION/DOWNGRADING SCHEDULE	
4. PERFORMING ORGANIZATION REPORT NUMBER(S): RADC-TR-84-215	5. MONITORING ORGANIZATION REPORT NUMBER(S)
6a. NAME OF PERFORMING ORGANIZATION: Rome Air Development Center — 6b. OFFICE SYMBOL (If applicable): RADC/EEAA	7a. NAME OF MONITORING ORGANIZATION
6c. ADDRESS (City, State and ZIP Code): Hanscom AFB Massachusetts 01731	7b. ADDRESS (City, State and ZIP Code)
8a. NAME OF FUNDING/SPONSORING ORGANIZATION — 8b. OFFICE SYMBOL (If applicable)	9. PROCUREMENT INSTRUMENT IDENTIFICATION NUMBER
8c. ADDRESS (City, State and ZIP Code)	10. SOURCE OF FUNDING NOS.: PROGRAM ELEMENT NO. 61102F; PROJECT NO. 2305; TASK NO. J3; WORK UNIT NO. 03
11. TITLE (Include Security Classification): Two-Degree-of-Freedom Linear and Planar Microwave Array Lenses	
12. PERSONAL AUTHOR(S): Daniel T. McGrath, Capt., USAF	
13a. TYPE OF REPORT: In-House — 13b. TIME COVERED: FROM ____ TO ____	14. DATE OF REPORT (Yr., Mo., Day): 1984 October — 15. PAGE COUNT: 36
16. SUPPLEMENTARY NOTATION	

17. COSATI CODES

FIELD	GROUP	SUB. GR.
09	03	

18. SUBJECT TERMS (Continue on reverse if necessary and identify by block number): Microwave lens; Lens antennas; Multiple-beam antennas; Electronically-scanned antenna; Low sidelobe antennas

19. ABSTRACT (Continue on reverse if necessary and identify by block number)

A new design of beamforming lens is presented. Both faces are planar arrays of microwave or millimeter wave antenna elements, interconnected by transmission lines (as in a "bootlace" lens) whose length vary as a function of radius. While the front face elements are regularly spaced, the back face elements are displaced radially from their corresponding front face elements, the amount of displacement also being a function of radius. Such a lens is shown to be capable of forming low sidelobe pencil beams over a solid angle of ± 25° or more by switching between clusters of only seven feed elements. Because both faces are planar, construction of extremely lightweight lenses for large-aperture and/or multiple-beam antennas is feasible.

20. DISTRIBUTION/AVAILABILITY OF ABSTRACT: UNCLASSIFIED/UNLIMITED ☐ SAME AS RPT. ☒ DTIC USERS ☐	21. ABSTRACT SECURITY CLASSIFICATION: Unclassified
22a. NAME OF RESPONSIBLE INDIVIDUAL: D. McGrath, Capt, USAF	22b. TELEPHONE NUMBER (Include Area Code): (617) 861-4036 — 22c. OFFICE SYMBOL: RADC/EEAA

DD FORM 1473, 83 APR — EDITION OF 1 JAN 73 IS OBSOLETE.

Unclassified

SECURITY CLASSIFICATION OF THIS PAGE

Contents

Illustrations

Illustrations

Tables

Two-Degree-of-Freedom Linear and Planar Microwave Array Lenses

1. INTRODUCTION

Although the Rotman lens is considered the optimum beamformer for producing time-delay steered beams over wide angles, its requirement of a curved back face prohibits application to some problems, most notably those requiring large planar arrays. For such systems the most practical lens antenna is one with two planar microstrip (or perhaps monolithic) arrays facing in opposite directions, whose elements are connected by transmission lines through their respective ground planes. Fabrication of such a lens would be straightforward, in contrast to a two-dimensional Rotman lens with its concave-spherical back face.

Yet a Rotman lens has three geometric "degrees of freedom:" the curvature of the back face; the difference in lateral positions of elements on front (aperture side) and back (feed side) faces; and the variable transmission line lengths connecting the two.[1] In retreating from that design in order to maintain planar surfaces, the unfortunate tendency is to discard not only the first, but the second degree of freedom as well. The result is a lens that can focus perfectly only at a single point, but more importantly one whose feed cannot scan even a few degrees off-axis without severe pattern distortion.

(Received for publication 10 October 1984)

1. Rotman, W., and Turner, R.F. (1963) Wide-angle microwave lens for line source applications, IEEE Trans. Antennas Propag., pp. 723-632.

This report will show that allowing the position of feed side elements to vary with respect to those on the aperture side yields substantially better performance in a lens whose front and back faces are both linear or planar. It will explain the general concept in terms of a two-dimensional (linear) lens and later extend that design to the planar case. In comparison to the one-degree-of-freedom approach it will show that phase errors can be reduced by two orders of magnitude, allowing synthesis of low-sidelobe patterns over an angular region eight times as large.

2. LINEAR LENS

2.1 Uniform Element Spacing

Under the constraint that both lens surfaces are flat, we will consider first the two-dimensional design depicted in Figure 1. In this case, the elements on opposing lens surfaces have the same lateral locations, that is $Y = N$, and are joined by transmission lines of varying length, W. Through the heuristic argument that there can be only as many perfect focal points as there are degrees of freedom we know this lens can only have one focus because its only degree of freedom is in the line lengths. But we can prove this by attempting to find a W(y) that yields two focal points, as follows:

The point source at ($F \cos \alpha$, $F \sin \alpha$) in Figure 1 is to produce a plane wave directed at an angle α from broadside. Hence the path length from that point to any point on the wavefront must be constant:

$$R_1 + W + N \sin \alpha = F + W_o . \tag{1}$$

We want the second point to produce a wavefront directed at $-\alpha$ and therefore

$$R_2 + W - N \sin \alpha = F + W_o . \tag{2}$$

The distances R_1 and R_2 are

$$R_1 = [F^2 + Y^2 - 2\, YF \sin \alpha]^{1/2} \tag{3}$$

$$R_2 = [F^2 + Y^2 + 2\, YF \sin \alpha]^{1/2} . \tag{4}$$

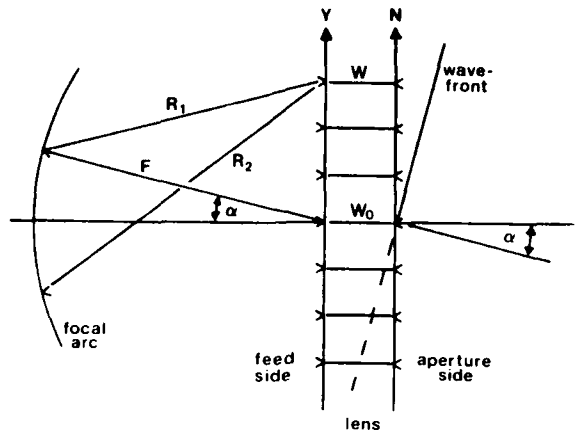

Figure 1. Linear Lens Geometry, One Degree of Freedom

Solving Eqs. (1) and (2) simultaneously with Y = N:

$$2\,Y \sin\alpha = [F^2 + Y^2 + 2\,YF \sin\alpha]^{1/2} - [F^2 + Y^2 - 2\,YF \sin\alpha]^{1/2} \qquad (5a)$$

$$2\,Y^2 \sin^2\alpha = F^2 + Y^2 - [F^4 + Y^4 + 2\,Y^2F^2 - 4\,Y^2F^2 \sin^2\alpha]^{1/2} \qquad (5b)$$

$$(F^2 + Y^2 - 2\,Y^2 \sin^2\alpha)^2 = F^4 + Y^4 + 2\,Y^2F^2 - 4\,Y^2F^2 \sin^2\alpha\,. \qquad (5c)$$

Carrying out the square on the left and simplifying leaves

$$\sin^4\alpha = \sin^2\alpha \qquad (6)$$

which can only be true if $\alpha = 90°$ (a useless case) or if $\alpha = 0$ (that is, one focal point).

2.2 Non-uniform Spacing

If we now allow the feed side elements to be at different lateral locations than those on the aperture side, as in Figure 2, or $Y \neq N$ then Eq. (5) becomes

$$2N \sin\alpha = [F^2 + Y^2 + 2\,YF \sin\alpha]^{1/2} - [F^2 + Y^2 - 2\,YF \sin\alpha]^{1/2} \qquad (7a)$$

$$2N^2 \sin^2\alpha = F^2 + Y^2 - [F^4 + Y^4 + 2\,Y^2F^2 - 4\,Y^2F^2 \sin^2\alpha]^{1/2}\,, \qquad (7b)$$

$$(F^2 + Y^2 - 2N^2 \sin^2\alpha)^2 = F^4 + Y^4 + 2\,Y^2F^2 - 4\,Y^2F^2 \sin^2\alpha\,, \qquad (7c)$$

$$N^4 \sin^2\alpha = Y^2N^2 + F^2N^2 - Y^2F^2 \qquad (7d)$$

and finally,

$$Y = N \left[\frac{F^2 - N^2 \sin^2 \alpha}{F^2 - N^2} \right]^{1/2} \tag{8}$$

which has solutions for all choices of α. Next, we solve Eqs. (1) and (2) for W:

$$W = F + W_o - \frac{1}{2} R_1 - \frac{1}{2} R_2$$

$$= F + W_o - \frac{1}{2} [F^2 + Y^2 - 2\,YF \sin \alpha]^{1/2} - \frac{1}{2} [F^2 + Y^2 + 2\,YF \sin \alpha]^{1/2} . \tag{9}$$

Equation (8) gives the position of feed side elements Y in terms of those on the aperture side, N. Then using Eq. (9) to find the line lengths completes the lens design, which will have two perfect focal points at angles α and $-\alpha$ at a distance F from the center of the lens.

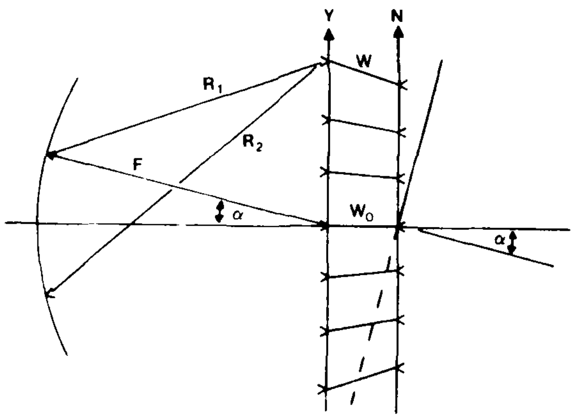

Figure 2. Linear Lens Geometry, Two Degrees of Freedom

Consistent with our heuristic argument, addition of the second-degree-of-freedom does indeed allow two perfect focal points. But of course the number of focal points is not our primary concern, but rather how well the lens focuses away from these points.

The best comparison between the two cases is in terms of the normalized path length error. In the first (Y = N) the path length from an arbitrary point on a focal arc of radius F to an aperture element is

$$L = W + R = F + W_0 - [F^2 + Y^2]^{1/2} + [F^2 + Y^2 - 2\,YF \sin \alpha]^{1/2} \tag{10}$$

while the desired path length is

$$\hat{L} = F + W_0 - N \sin \alpha . \tag{11}$$

The path length error normalized to the focal length with Y = N is

$$\frac{\epsilon}{F} = \frac{\hat{L} - L}{F} = (1 + y^2)^{1/2} - (1 + y^2 - y \sin \alpha)^{1/2} - y \sin \alpha \tag{12}$$

where $y = Y/F$. Figure 3 shows ϵ/F vs y for various choices of α. To put these errors in perspective, when $\alpha = 5°$ the error at $y = 0.6\,F$ is $0.007\,F$. For a lens whose focal length is a mere 10 wavelengths that translates into a phase error of 25.2°. Figures 4a, b, and c show the progressive degradation in the quality of beams produced by sources at $\alpha = 0°$, $2.5°$, and $5°$ along the focal arc using example parameters of $F = L = 200\lambda$ (L is the lens diameter) and element spacing of 3.41λ.

In the second case, $Y \neq N$, the desired path length L is the same as Eq. (11) but the actual path length is

$$L = F + W_0 + [F^2 + Y^2 - 2\,YF \sin \alpha]^{1/2}$$
$$- \frac{1}{2}[F^2 + Y^2 - 2\,YF \sin \beta]^{1/2} - \frac{1}{2}[F^2 + Y^2 + 2\,YF \sin \beta]^{1/2} \tag{13}$$

where α is the angle of the source and β is the chosen angle of perfect focus. Figure 5 shows that even when β is chosen as 0° (that is, a single focal point) the error associated with the innermost beams is reduced tremendously compared with Figure 3. Figure 6 shows the improvement in beam quality for $\alpha = 2.5°$, $5°$, and $7.5°$, again with the parameters $F = L = 200\lambda$ and $l = 3.41\lambda$. Figure 7 shows the path length errors resulting from perfect focusing at $\pm 15°$. The improvement of the outer beams ($\alpha = 30°$, $45°$) is about the same as the degradation of the inner beams) $\alpha = 0°$, $5°$).

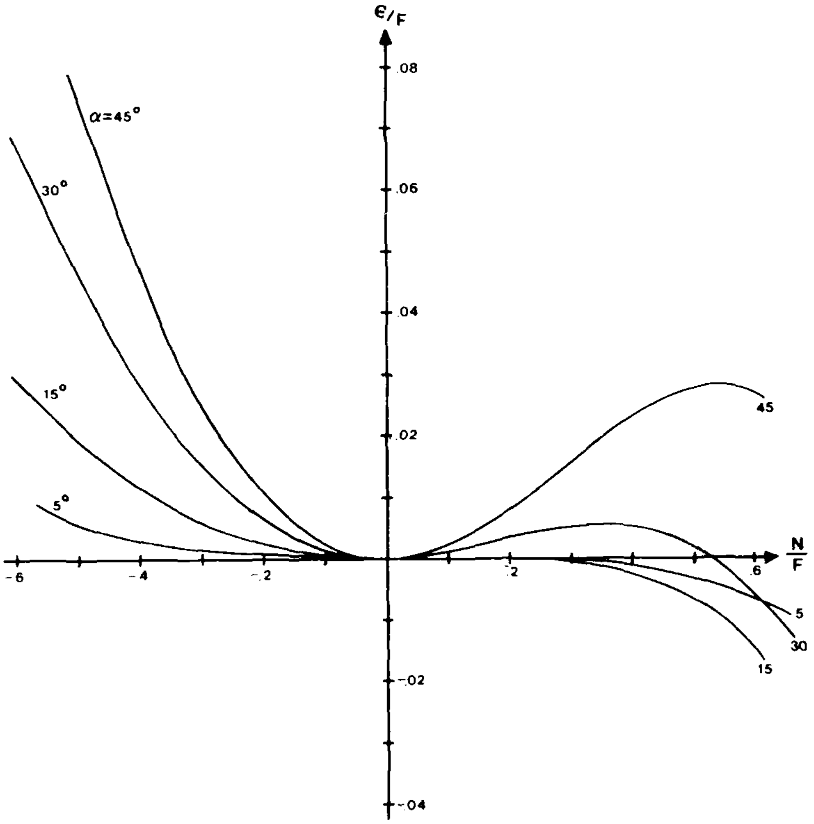

Figure 3. Normalized Path Length Error, Y = N

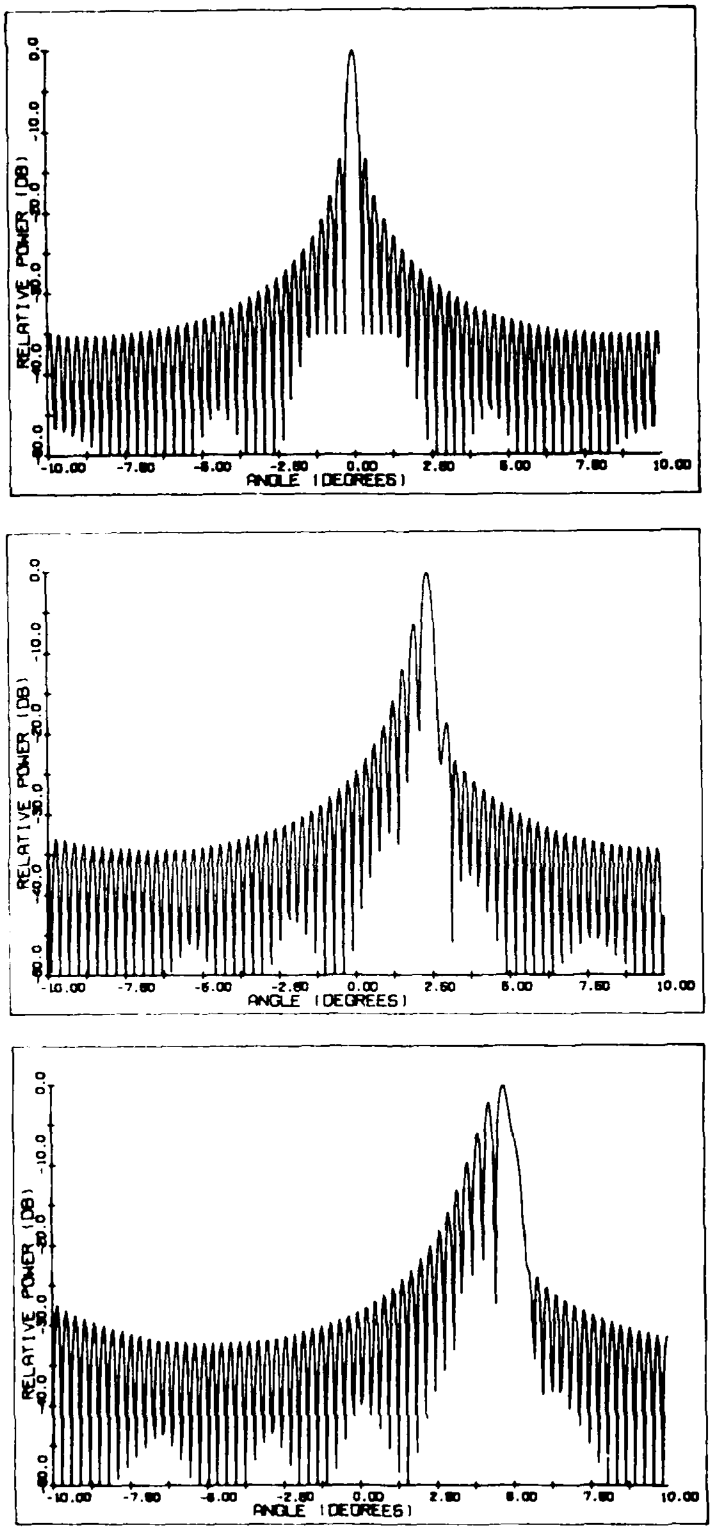

(a)

(b)

(c)

Figure 4. Defocusing in Off-Axis Beams

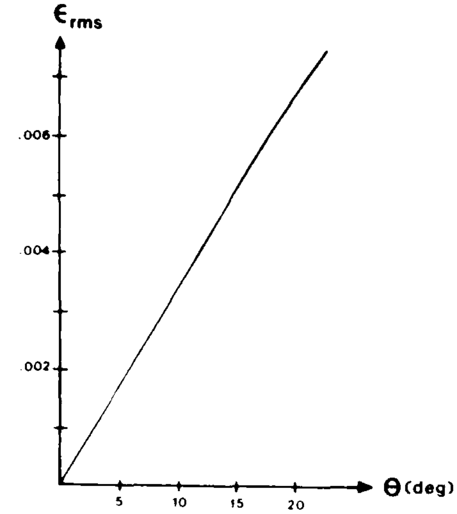

Figure 17. rms Path Length Error vs θ, 1 D.O.F.

3.2 Two-Degree-of-Freedom With Rotational Symmetry

Next, the radial positions of elements on the lens faces are allowed to vary according to Eq. (8):

$$\rho = p \left[\frac{1 - p^2 \sin^2 \theta_0}{1 - p^2} \right]^{1/2} . \tag{24}$$

From Eq. (9) the normalized line lengths are

$$w = 1 - \frac{1}{2} [1 + \rho^2 - 2\rho \sin \theta_0]^{1/2} - \frac{1}{2} [1 + \rho^2 + 2\rho \sin \theta_0]^{1/2} . \tag{25}$$

Since the distance from a beam port to the lens' back face elements is still given by Eq. (19) the actual path length to an aperture element is

$$\ell = [1 + \rho^2 - 2\rho \sin \theta \cos(\phi_\ell - \phi)]^{1/2} + 1$$

$$- \frac{1}{2} [1 + \rho^2 - 2\rho \sin \theta_0]^{1/2} - \frac{1}{2} [1 + \rho^2 + 2\rho \sin \theta_0]^{1/2} \tag{26}$$

while the desired length is the same as Eq. (20). The path length error is then

$$\epsilon = [1 + \rho^2 - 2\rho \sin \theta \cos(\phi_\ell - \phi)]^{1/2} + p \sin \theta \cos(\phi_\ell - \phi)$$

$$- \frac{1}{2} [1 + \rho^2 - 2\rho \sin \theta_0]^{1/2} - \frac{1}{2} [1 + \rho^2 + 2\rho \sin \theta_0]^{1/2} . \tag{27}$$

With the lens perfectly focused at $\theta_0 = 0$

$$W - W_0 = F - R = F - (F^2 + \rho^2 F^2)^{1/2} \tag{21}$$

and the actual path length is

$$L = R + W = R + F + W_0 - (F^2 + \rho^2 F^2)^{1/2} \tag{22a}$$

$$\ell = \frac{L}{F} = [1 + \rho^2 - 2\rho \sin\theta \cos(\phi_\ell - \phi)]^{1/2} + 1 + w_0 - [1 + \rho^2]^{1/2} . \tag{22b}$$

If $\rho = \rho$ and $\phi_a = \phi_\ell$ (same element positions on both lens faces) then the normalized path length error is

$$\epsilon = \ell - \hat{\ell} = [1 + \rho^2 - 2\rho \sin\theta \cos(\phi_\ell - \phi)]^{1/2} - [1 + \rho^2]^{1/2} + \rho \sin\theta \cos(\phi_\ell - \phi) . \tag{23}$$

Figure 16 is a contour plot of ϵ over an aperture whose diameter is $D = F$ when $\theta = 5°$. Figure 17 shows the rms error integrated over the aperture vs off-axis position (θ) of the beam port.

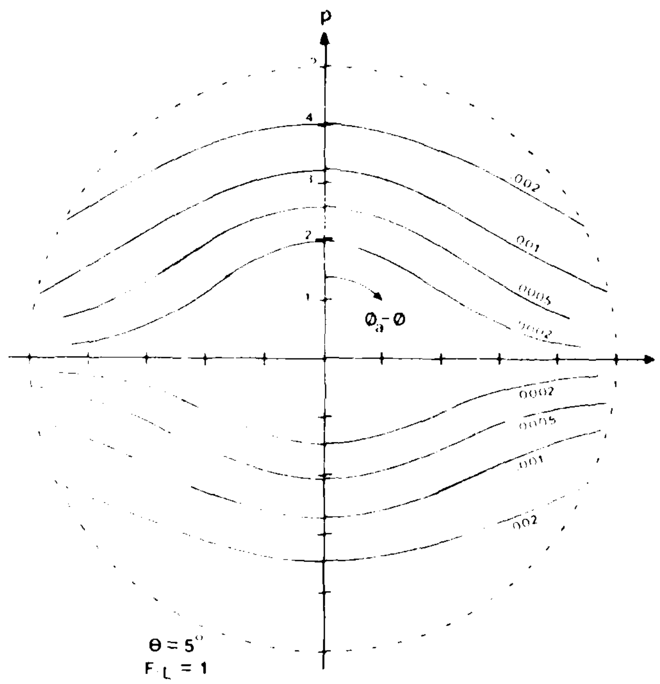

Figure 16. Path Length Error Contours, 1 D.O.F., $\theta = 5°$

3. PLANAR LENS

Extending the preceding design to a planar lens, one might hope to get more than two focal points. Certainly three should be possible since there are two degrees of freedom in either x and y or ρ and ϕ, plus a third in w. However we will neglect variation in ϕ and show instead a rotationally symmetric two-degree-of-freedom design which yields substantially better off-axis focusing than the similar one-degree-of-freedom design.

3.1 Single-Degree-of-Freedom Planar Lens

Figure 15 is the generalized planar lens geometry with normalized coordinates (ρ, ϕ_a) and (ρ, ϕ_ℓ) on aperture and feed sides respectively. Beam ports are located on a sphere of radius F whose center is at r = 0. The normalized coordinates of any point on the sphere are $(x_f, y_f, z_f) = (\sin\theta \cos\phi, \sin\theta \sin\phi, -\cos\theta)$. The distance from the beam port to an arbitrary point on the lens' feed side is

$$r = \frac{R}{F} \left[1 + \rho^2 - 2\rho \sin\theta \cos(\phi_\ell - \phi)\right]^{1/2} \tag{19}$$

and the desired path length to any aperture element is

$$\hat{\ell} = \frac{\hat{L}}{F} = 1 + w_0 - \rho \sin\theta \cos(\phi_a - \phi) \, . \tag{20}$$

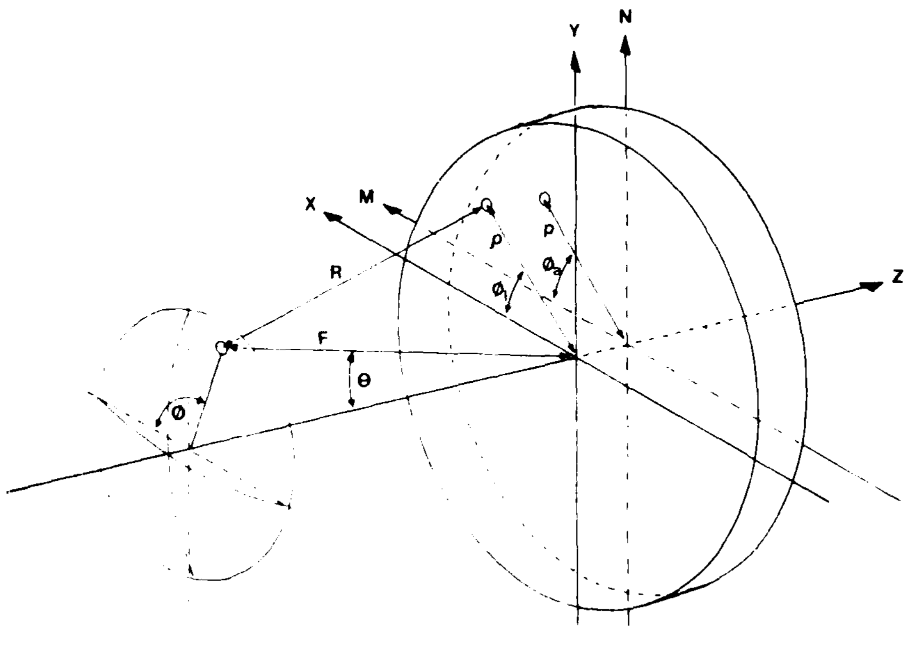

Figure 15. Reference Geometry, Planar Lens

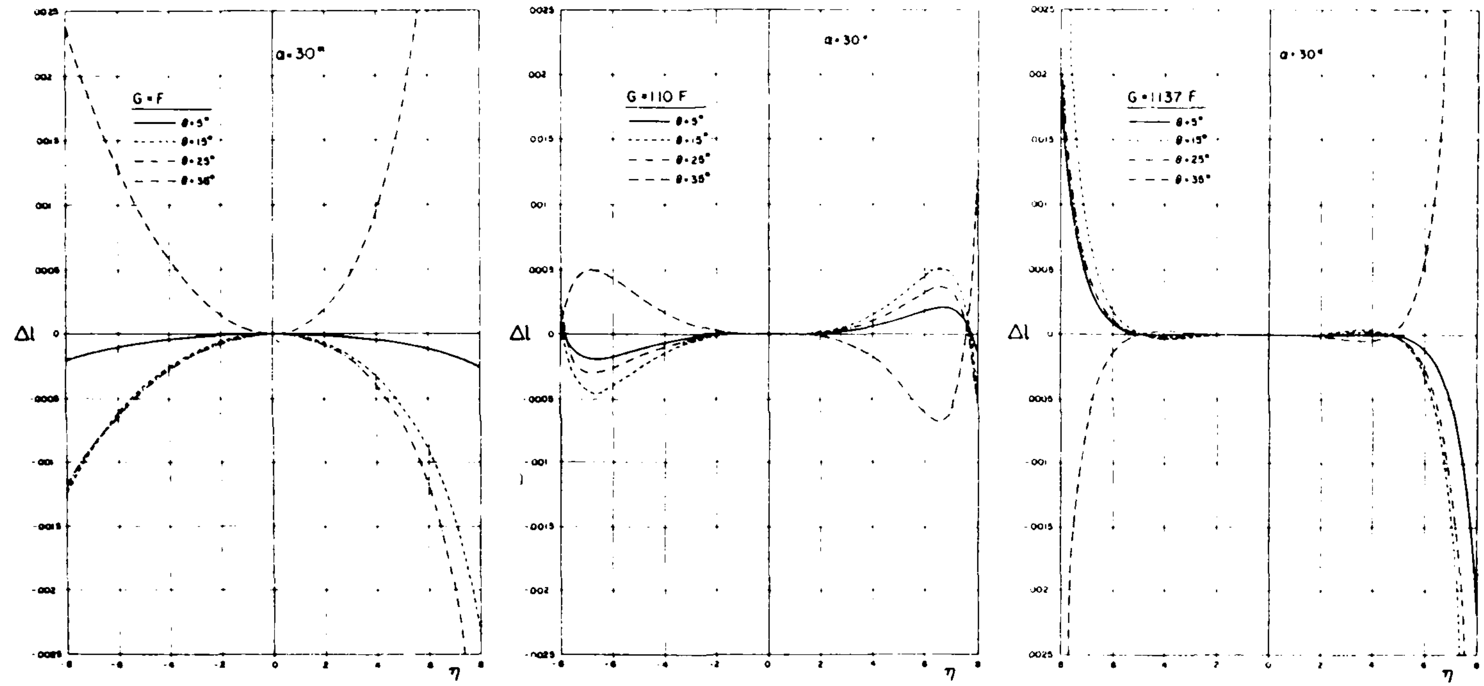

Figure 14. Rotman Lens Path Length Error

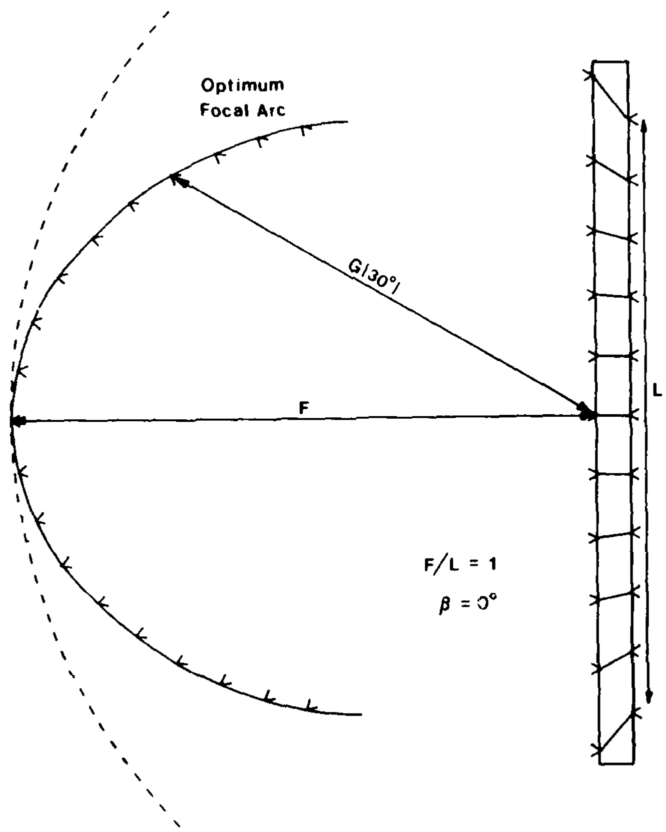

Figure 13. Optimum Focal Arc, $Y \neq N$, $\beta = 0$

We have studied the case where $F/D = 1$ in some detail and list $G(\alpha)$ for various choices of β in Table 1. These are those values of $G(\alpha)$ which minimize the root-mean-square (rms) path length error over the entire aperture. Figure 13 shows the shape of the optimum focal arc when $\beta = 0$. A good approximation is $G(\alpha) \approx F \cos\alpha / \cos\beta$.

Table 1. Distance $G(\alpha)$ From Lens Centerpoint of Refocused Beam Port for $F/D = 1$

	$G(\alpha)/F$				
$\alpha°$	$\beta = 0$	$\beta = 5°$	$\beta = 10°$	$\beta = 15°$	$\beta = 20°$
0	1.000	1.006	1.025	1.059	1.108
2.5	0.998	1.005	1.024	1.057	1.106
5	0.994	1.000	1.019	1.052	1.100
7.5	0.986	0.992	1.011	1.043	1.091
10	0.976	0.982	1.000	1.031	1.078
12.5	0.963	0.969	0.987	1.017	1.062
15	0.949	0.954	0.971	1.000	1.043
17.5	0.932	0.937	0.953	0.981	1.023
20	0.914	0.919	0.934	0.961	1.000
22.5	0.895	0.899	0.914	0.939	0.976
25	0.875	0.879	0.893	0.916	0.951
27.5	0.854	0.858	0.871	0.893	0.925
30	0.833	0.837	0.849	0.869	0.899
32.5	0.811	0.815	0.826	0.845	0.873
35	0.790	0.793	0.803	0.821	0.847
37.5	0.768	0.771	0.780	0.797	0.821
40	0.746	0.749	0.758	0.773	0.795
42.5	0.725	0.727	0.735	0.749	0.769
45	0.703	0.705	0.713	0.725	0.744
47.5	0.682	0.684	0.690	0.702	0.719
50	0.660	0.662	0.668	0.679	0.694

As a final comparison, Figure 14c from Rotman and Turner[1] shows the path length error in an optimally refocused Rotman lens. Although our two-degree-of-freedom design cannot match that result it is still two orders of magnitude better in terms of path length error than the N × N design.

2.5 Beam Port Refocusing

There is yet one further improvement we could make in the lens design. Note that in Figures 5 and 7 the path length errors tend to be quadratic, in contrast to Figure 3, in which they are cubic. The second-order quadratic error can be suppressed by "refocusing" the beam ports, that is moving them closer to, or farther away from the lens while maintaining their angular positions.

For Figure 12 the angle of perfect focus, β, was chosen at 15°, and the figure shows how the error associated with the on-axis beam port ($\alpha = 0$) varies as it is moved away from the lens. Clearly, the ideal position depends on the aperture length: if $N_{max} = 0.6\,F$ then G should be $1.05\,F$; if $N_{max} = 0.4\,F$ then $G = 1.065\,F$ is better.

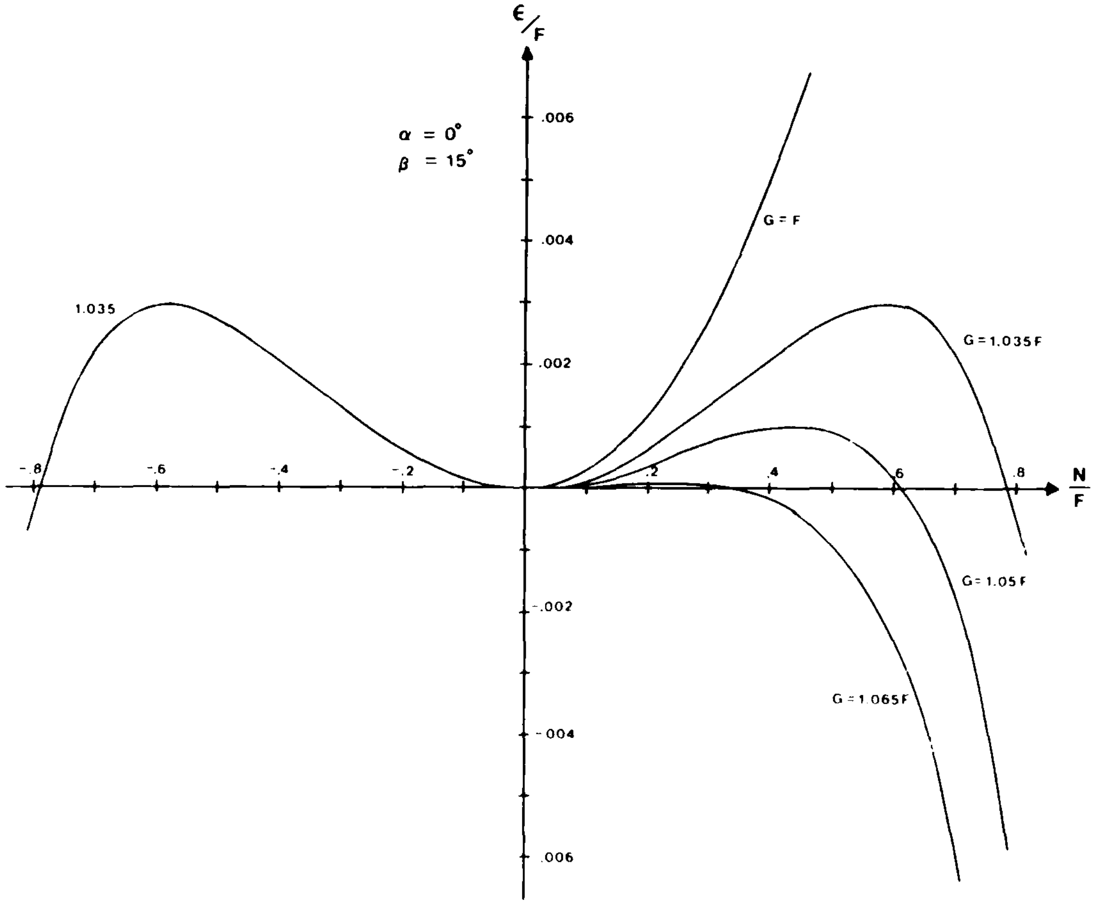

Figure 12. Path Length Error With Refocusing, $Y \neq N$, β 0

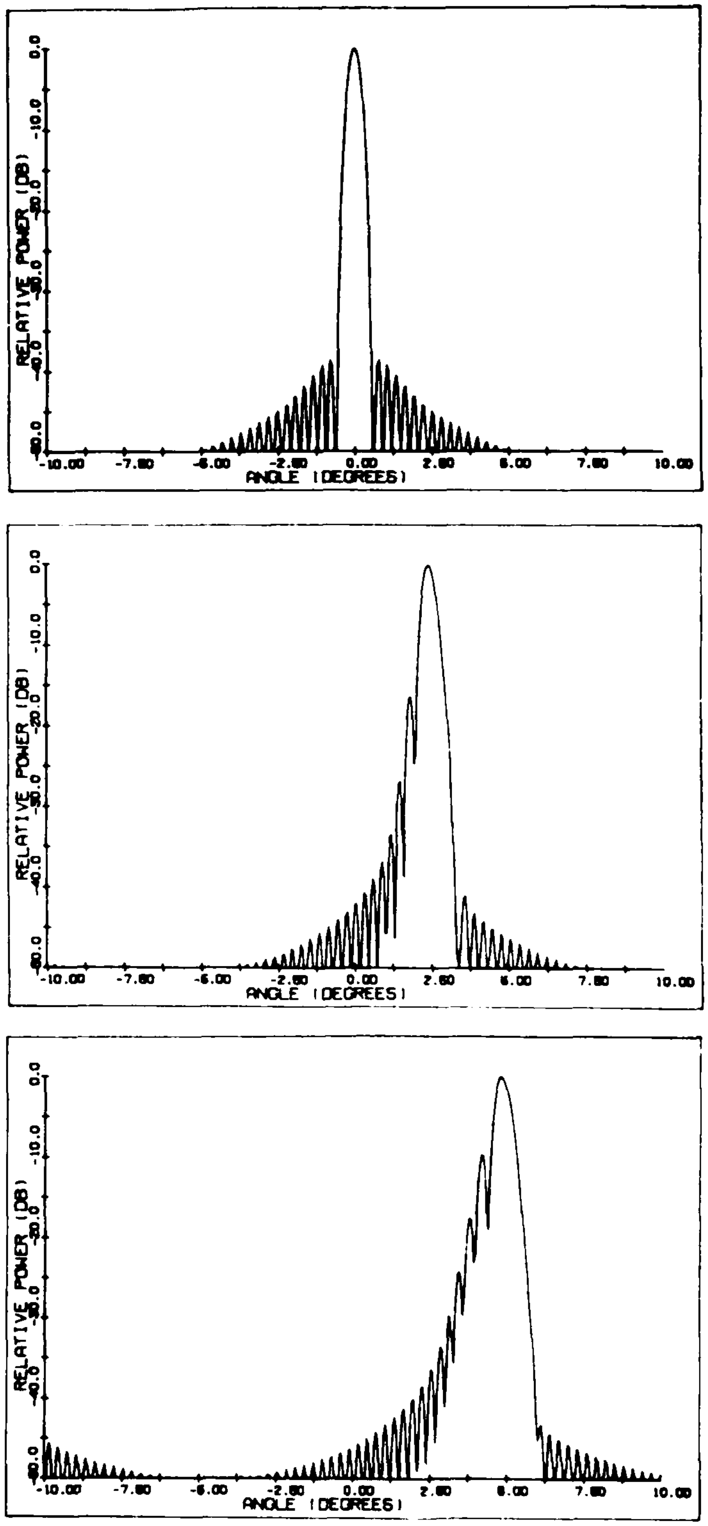

(a)

(b)

(c)

Figure 11. Synthesized Patterns, One-Degree-of-Freedom Lens

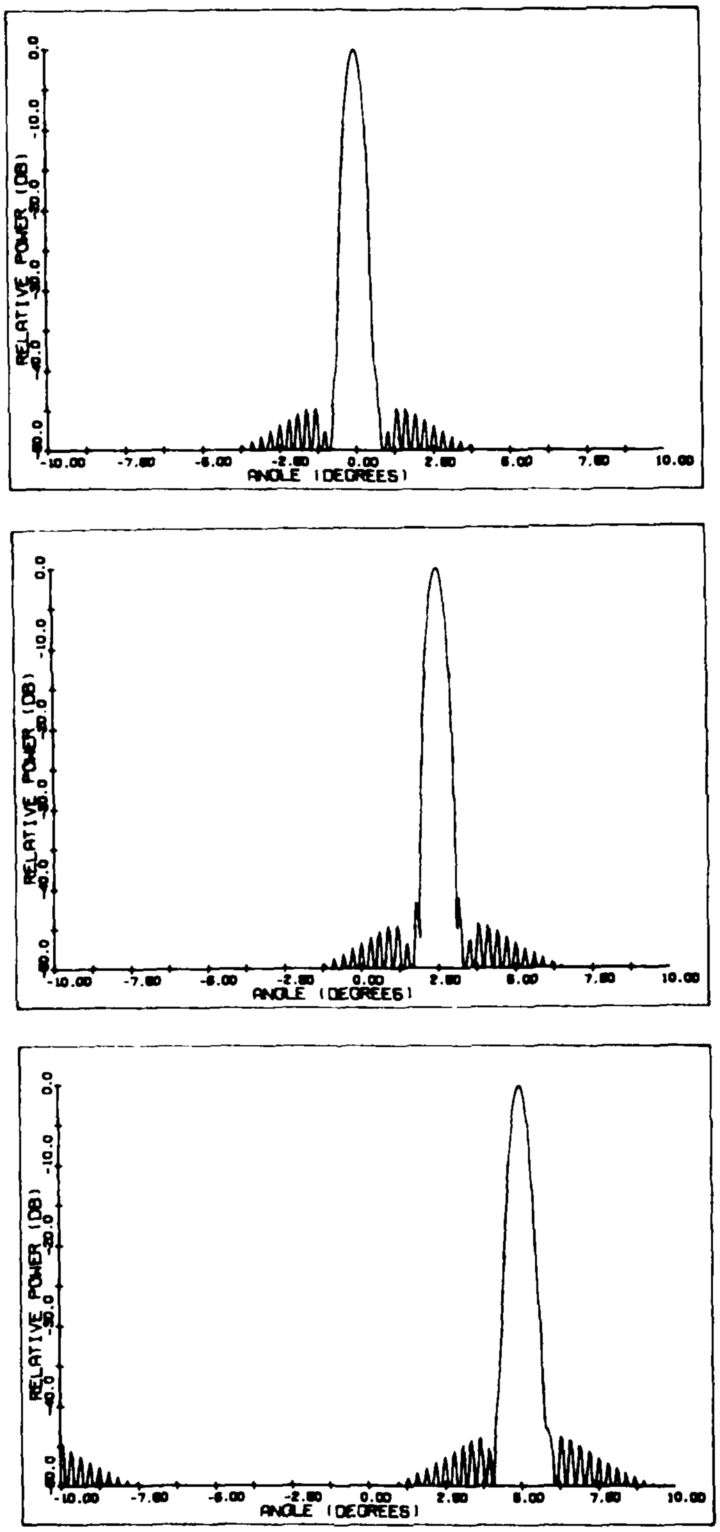

(a)

(b)

(c)

Figure 10. Synthesized Low-Sidelobe Patterns, Two-Degree-of-Freedom Lens, $\beta = 2.5°$

2.4 Pattern Synthesis

White[3] discusses pattern synthesis with multiple-beam antennas. The technique is fairly straightforward when the beams produced by each feed are orthogonal, which in the case of sin(x)/x beams implies that each beam peak coincides with the first nulls of adjacent beams.

For example, assuming parameters $F = L = 200\lambda$, the beamwidth is 0.3°. Then the beam ports should be spaced at 0.3° intervals along the focal arc. If we now want to create a Hamming window aperture distribution, we refer to Figure 9 showing the Fourier transforms of the rectangular and Hamming windows. At the first null of the rectangular, the Hamming is -7.41 dB. Therefore, the correct amplitude weights for a three-element subarray are -7.41 dB, 0.0 dB, -7.41 dB.

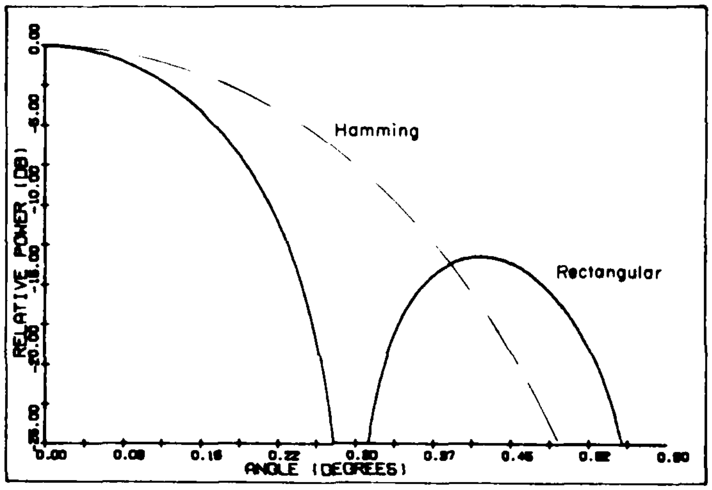

Figure 9. Rectangular and Hamming Window Transforms

We have chosen the Hamming distribution because it can be produced using a small number of feed elements. Distributions such as the Dolph Chebyshev or the Taylor will in general require a large number of feed elements and consequently elaborate beam-switching networks. Appendix A shows that given only three beam ports, the Hamming window gives the lowest peak sidelobes.

Figures 10a, b, and c show the (error-free) patterns produced by the two-degree-of-freedom linear lens focused at ± 2.5° when the subarray is centered at 0°, 2.5°, and 5°, respectively. Figures 11a, b, and c show the attempt to do the same with a Y - N lens: even with the subarray on-axis, path length errors in the ± 0.30° beams are sufficient to raise the near-in sidelobes by about 5 dB.

3. White, W. D. (1962) Pattern limitations in multiple-beam antennas, IEEE Trans. Antennas and Propag., pp. 430-436.

In the two-degree-of-freedom design with both perfect focal points on axis

$$Y = \frac{NF}{\sqrt{F^2 - N^2}} = F \tan \gamma \, . \tag{15}$$

By the identity

$$\tan \gamma = \frac{\sin \gamma}{\sqrt{1 - \sin^2 \gamma}} \, , \tag{16}$$

$$\frac{N}{\sqrt{F^2 - N^2}} = \frac{F \sin \gamma}{\sqrt{F^2 - F^2 \sin^2 \gamma}} \tag{17}$$

which implies that

$$N = F \sin \gamma \tag{18}$$

which satisfies the Abbe condition identically with $f = F$. Hence, a classical optics analysis verifies what we have already established: that this lens is capable of limited feed displacement without significant defocusing.

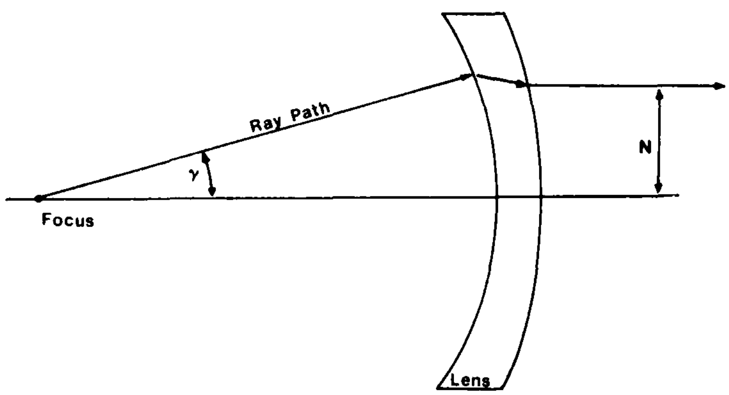

Figure 8. Sine Condition Geometry

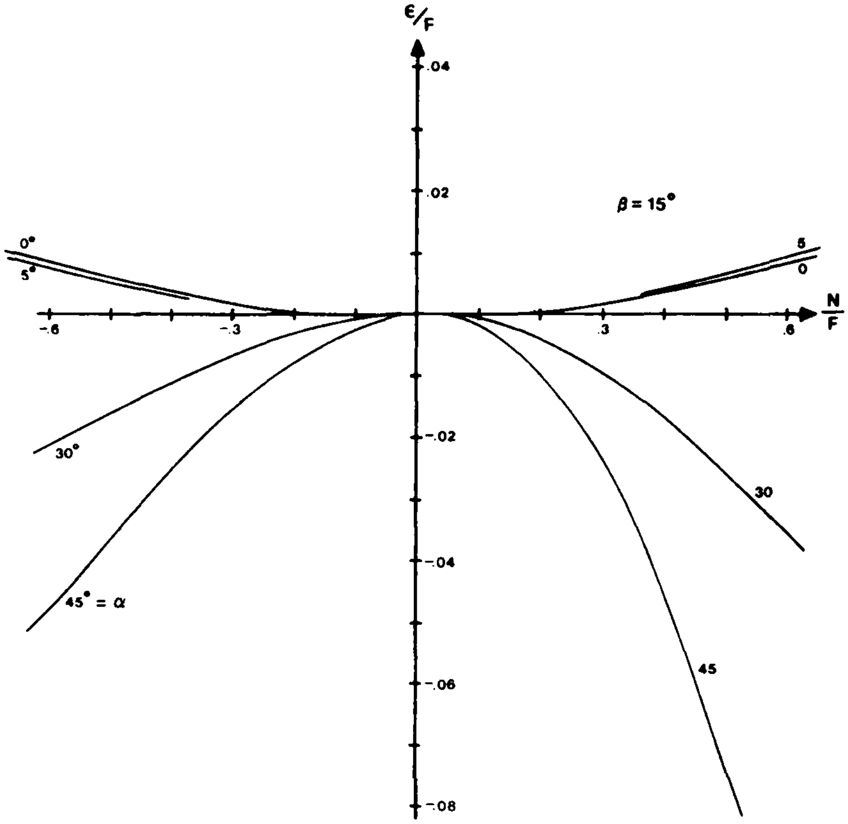

Figure 7. Normalized Path Length Error, $Y \neq N$, $\beta = 15°$

2.3 The Sine Condition

A well-known theorem of geometrical optics known as the "Abbe sine condition"[2] states that in order for a lens to focus off-axis the lateral coordinate N at which a ray from the on-axis focus exits the aperture must equal a constant f times $\sin\gamma$ where γ is the angle between the lens axis and the ray from the focus to the back lens face as shown in Figure 8.

$$N = f \sin\gamma . \tag{14}$$

2. Born, Max, and Wolf, Emil (1964) Principles of Optics, Pergamon Press, Oxford, England.

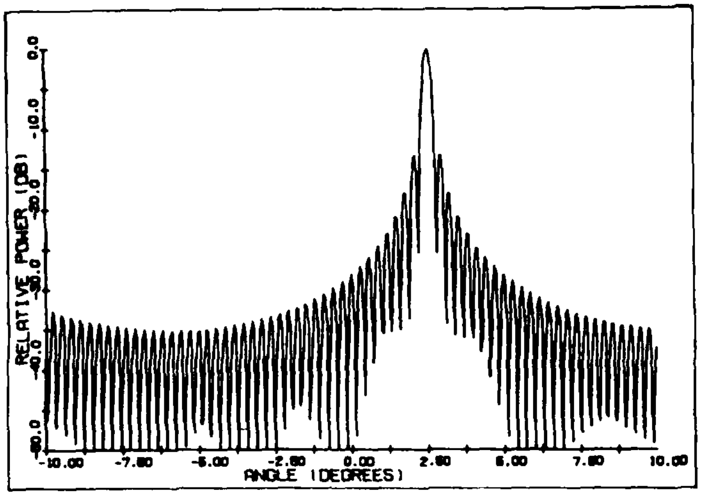

(a)

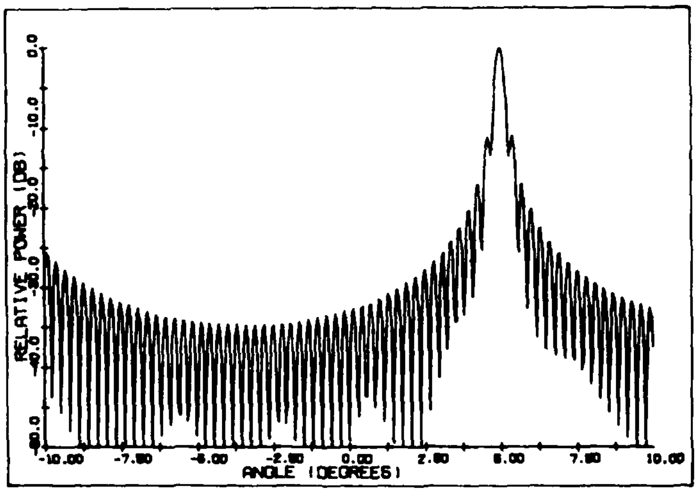

(b)

Figure 6. Improved Off-Axis Beams

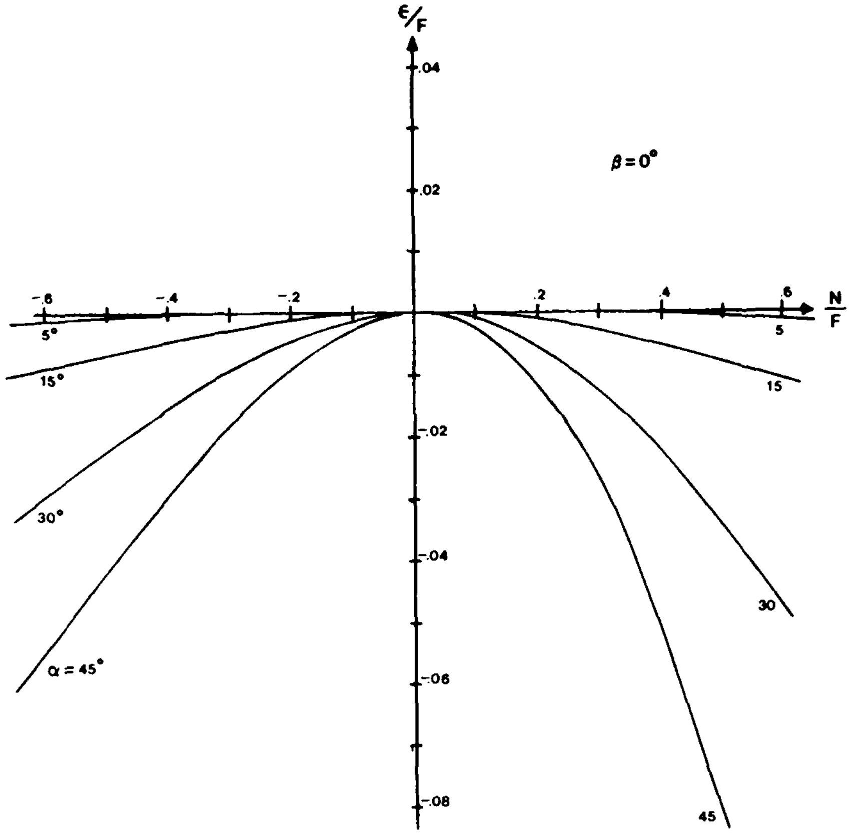

Figure 5. Normalized Path Length Error, Y ≠ N, β = 0°

If we choose $\theta_o = 0$ for perfect focus at broadside we get the error levels shown in Figure 18, again for $\theta = 5°$ and $F/D = 1$. In comparison to Figure 16 the magnitude of the error is reduced by a factor of 10. Furthermore it is approximately constant along any line parallel to $(\varphi_\ell - \theta) = 90°$, indicating that the beam is perfectly focused in the φ-plane perpendicular to that containing the beam port.

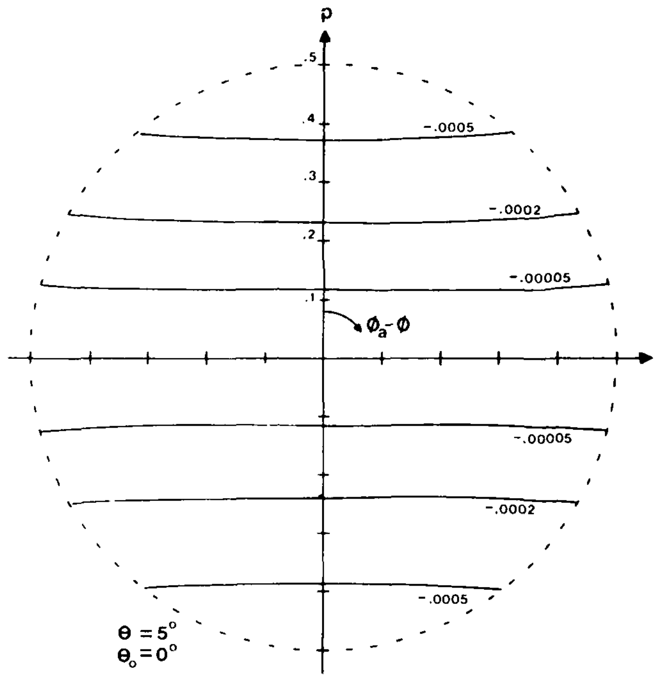

Figure 18. Path Length Error Contours, 2 D.O.F., $\theta = 5°$, $\theta_o = 0$

When we set $\theta_o = 5° = \theta$, attempting to focus off-axis, we get errors identical to those shown in Figure 18, except rotated 90°. In other words, the overall focusing is not improved, but perfect focusing is achieved in the beam's own φ-plane rather than the one perpendicular to it.

In Figure 19 the rms path length error is shown vs θ for several choices of θ_o. It is always minimum at $\theta = \theta_o$, but for $\theta_o > 5°$ the degradation in beams inside θ_o is appreciably worse than the improvement in beams outside θ_o. This suggests that in most cases there is no real advantage in attempting to focus off-axis.

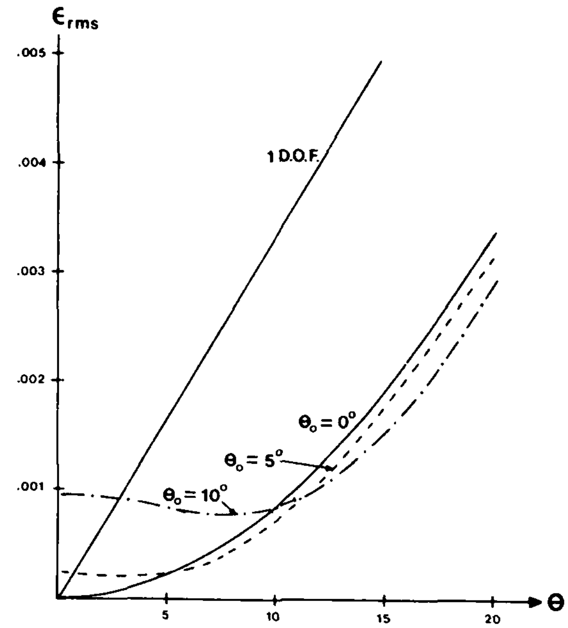

Figure 19. rms Path Length Error vs θ, 2 D.O.F.

Again, refocusing of the beam ports is possible, but the values of Table 1 do not apply. For example with $\theta_0 = 0$ and $\theta = 5°$, Table 1 gives $G(\theta = 5°) = 0.994$, but the resulting error contours are not very much different from Figure 18 save that they are rotated 90°—refocusing in one direction ($\phi = 0$) destroys the focusing at $\phi = 90°$. In this case it turns out that the best choice of G is 0.997, with error contours shown in Figure 20. This does appreciably reduce the rms error because the contour values are lower than those in Figure 18, but the beam is no longer perfectly focused in any plane of ϕ. In general the best choice of G is that which makes the error minimum along a contour $(\phi_\ell - \phi) = \pm 45°$.

3.3 Two-Degree-of-Freedom Simulation

Synthesizing a low sidelobe pattern in three dimensions using a lens is similar to the technique discussed in Section 2.3, but the feed is a seven-element subarray in an equilateral-triangular lattice. When the array is shifted off-axis (see Figure 21) to some other point on the focal sphere of radius F, the coordinates of the outer elements are (found by inspection)

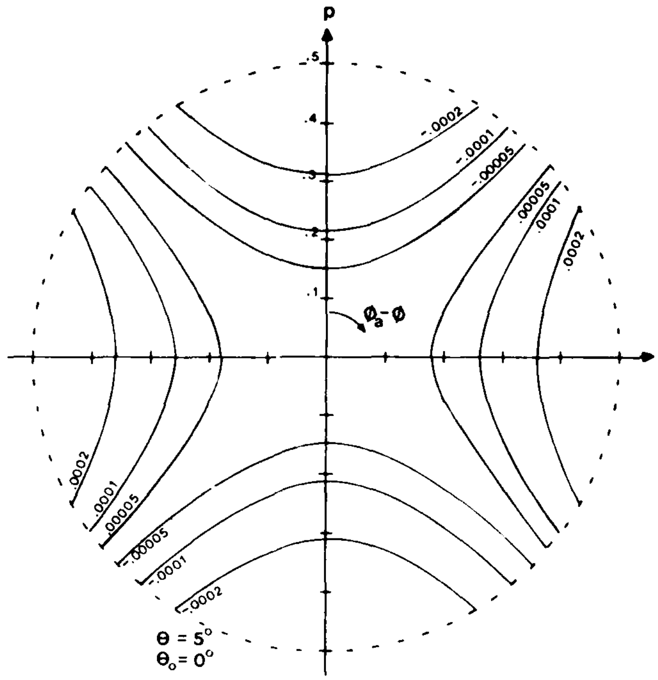

Figure 20. Path Length Error Contours With Refocusing

$$\phi_n = \tan^{-1}\left\{\frac{\sin\theta_3 \sin\psi_n}{\sin\theta_0 + \cos\theta_0 \cos\psi_n \quad \sin\theta_3}\right\} + \phi_0 \tag{28}$$

$$\theta_n = \frac{\theta_0 + \theta_3 \cos\psi_n}{\cos\phi_n} \tag{29}$$

where θ_o, ϕ_o are the coordinates of the center element and θ_3 is the beamwidth of the aperture. The angle ψ_n takes on values $n \times 60°$ and is measured from the direction of ϕ_o. The geometry of the subarray, viewed from the +z direction is Figure 21. Appendix A shows that for this feed geometry, with a circular aperture, the outer six elements should be weighted -9.87 dB relative to the center element.

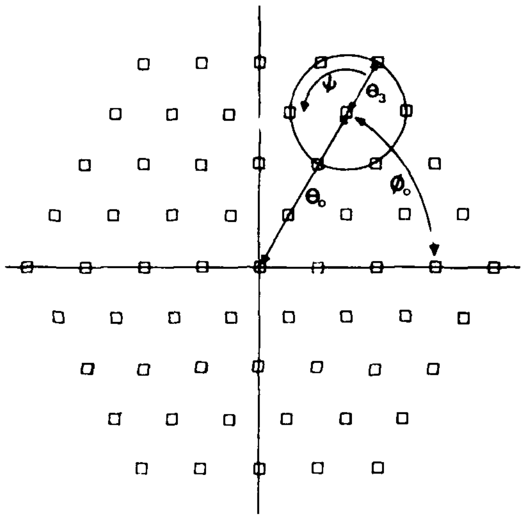

Figure 21. Subarray Geometry for 2D Lens Feed

The beamwidth of a circular aperture of diameter D is approximately 1.22 times that of a square aperture of width D,[4] or:

$$\theta_3 \approx 70^\circ \frac{\lambda}{D} \sec \theta_0 . \qquad (30)$$

We have chosen to simulate a lens whose aperture diameter and focal length are both 70 wavelengths with aperture elements spaced 3.41 λ apart in an equilateral lattice.

Figures 22a-d are the patterns of a one-degree-of-freedom lens with the feed displaced 0°, 2.5°, 5°, and 7.5° off-axis in azimuth, showing the rise of coma-error lobes on the side of the main beam nearest broadside. At 2.5° of scan the first lobe is already above -30 dB relative to the beam peak. By contrast, the patterns of the two-degree-of-freedom lens (with perfect focus at broadside) shown in Figures 23a-d show no appreciable degradation out to about 10° off-axis. Even at 12.5° (Figure 22d) there is little change in the $\phi = 0°$, 60°, and 120° planes, but nulls in the $\phi = 30°$, 90°, and 150° planes are filled in.

---

4. Goodman, J. W. (1968) Introduction to Fourier Optics, McGraw-Hill.

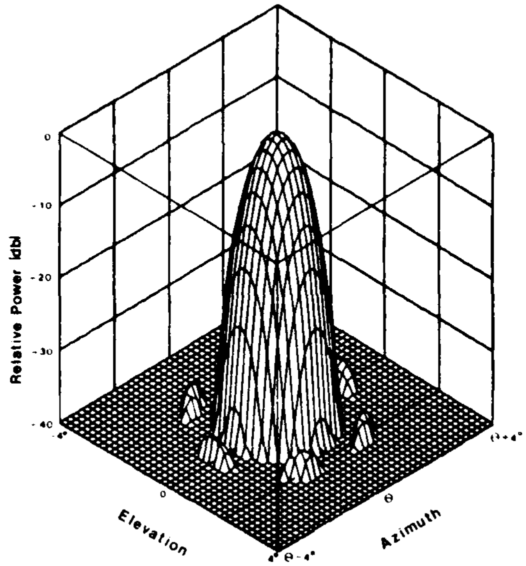

(a) θ = 0°

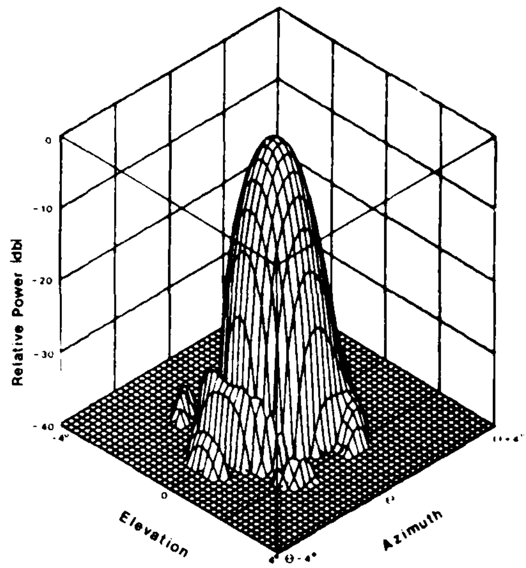

(b) θ = 2.5°

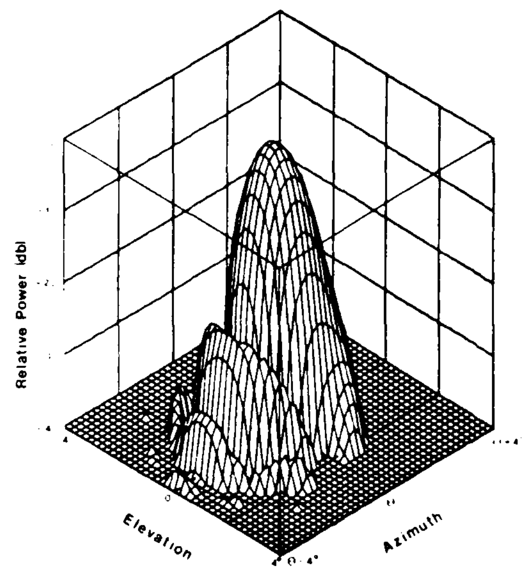

(c) θ = 5.0°

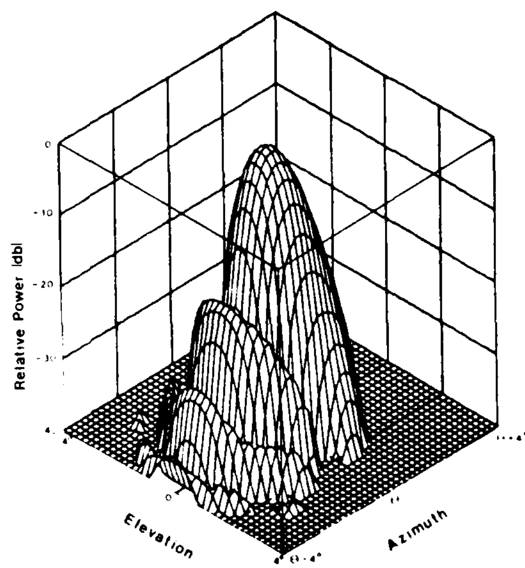

(d) θ = 7.5°

Figure 22. Synthesized Patterns, 1 D.O.F. Planar Lens

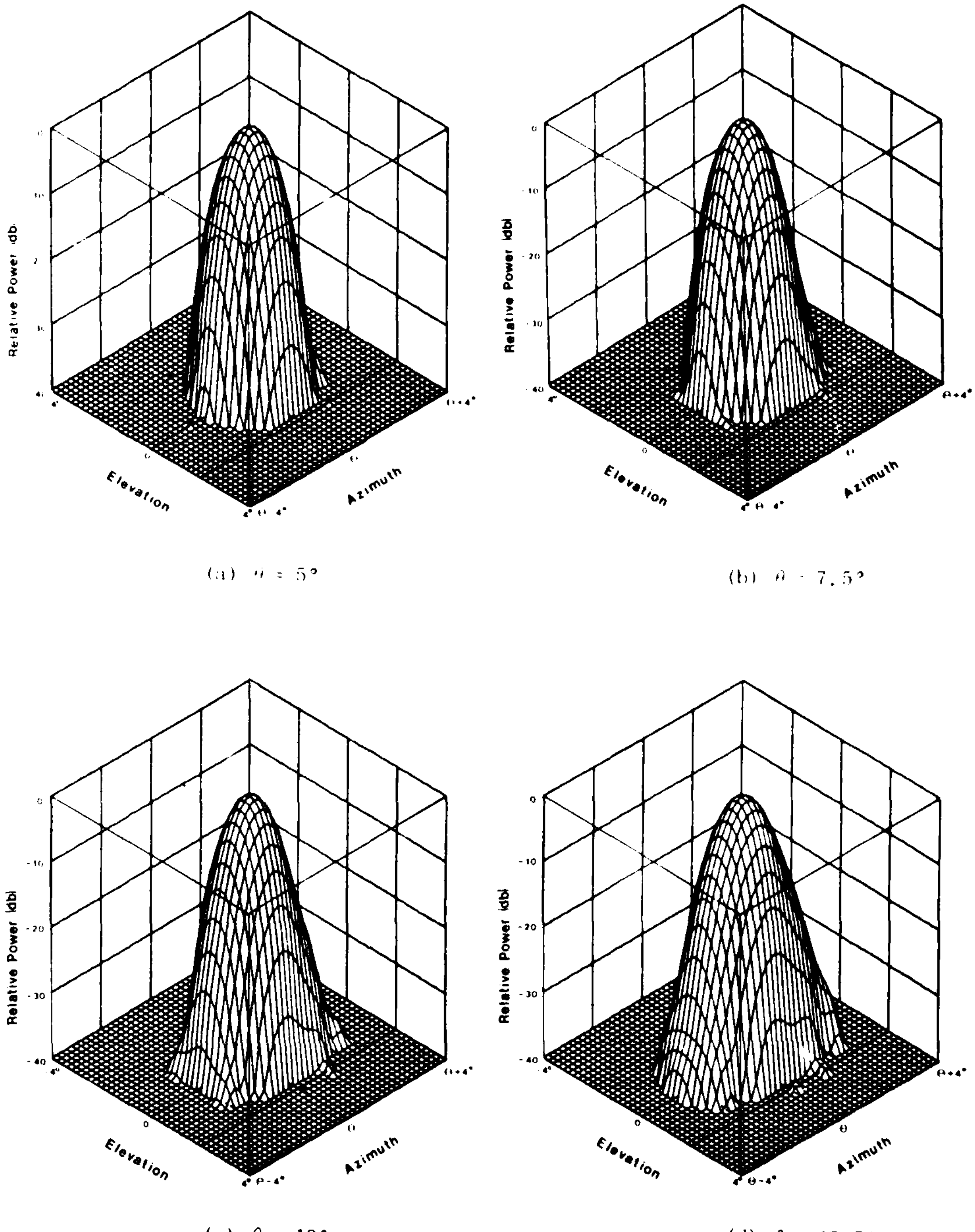

Figure 23. Synthesized Patterns, 2 D.O.F. Planar Lens

3.4 Proposed Experimental Model

The experimental model we propose consists of two planar arrays of edge-fed rectangular microstrip patches. The arrays, facing in opposite direction, have a common ground plane. Their elements will be interconnected through the ground plane as shown in Figure 24. Elements on the two faces are cross-polarized to reduce spillover effects. Meander lines are used to achieve the desired line lengths, s, for the chosen focal length. This figure illustrates the potential simplicity of fabrication of such a lens, with a tremendous reduction in weight over dielectric or waveguide lenses.

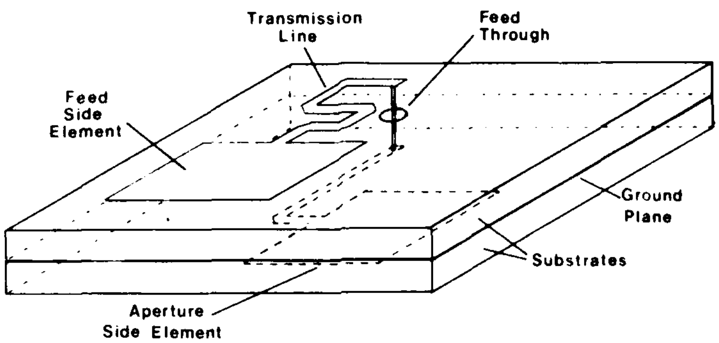

Figure 24. Proposed Experimental Model Element Design

4. CONCLUSIONS AND RECOMMENDATIONS

We have shown that a two-degree-of-freedom lens in which positions of aperture and feed side elements are different allows substantially better off-axis performance than the single-degree-of-freedom design. It allows synthesis of low-sidelobe patterns out to ± 10° from broadside or better with a very small number of feed elements. Although its focusing properties cannot match those of a Rotman lens, both faces of the lens are planar, which will make fabrication easier, particularly for very large aperture antennas.

The planar lens design described here uses only two of a possible three degrees of freedom since variation of element positions in radius only is allowed. Variation in angle φ may yield still better performance, and should be studied. Because of its potential application to limited-scan antennas, most notably multiple-beam satellite communications antennas, fabrication and test of a prototype lens is recommended.

Appendix A

Synthesis of Low-Sidelobe Aperture Distributions for Lens Antennas With a Small Number of Feed Elements

A1. TWO-DIMENSIONAL LENS

When a perfectly-focusing lens is illuminated by a subarray of (N - 1) elements located at orthogonal angles along its focal arc, the aperture distribution will have the form

$$A(x) = \sum_{n=0}^{N/2-1} b_n \cos(n\pi x/a) . \tag{A1}$$

The length of the array forming the aperture is 2a. The amplitude weights of the subarray elements are, for n = 1-N/2, ..., 1, 0, 1, ..., N/2-1 (N is odd), b_n = ..., 1/2 b_2, 1/2 b_1, b_0, 1/2 b_1, 1/2 b_2, ..., that is only symmetric distributions are considered. Effects of feed and/or lens element patterns are neglected.

The far field pattern is the Fourier transform of A(x):

$$f(u) = 2 \sum_{n=0}^{N/2-1} \frac{b_n u(-1)^n \sin(ua)}{u^2 - (n\pi/a)^2} . \tag{A2}$$

If we allow only three element subarrays then Eq. (A2) reduces to (with $b_0 = 1$):

$$f(u) = 2\,\frac{\sin(ua)}{u} + 2b_1\,\frac{u \sin(ua)}{(\pi/a)^2 - u^2} . \tag{A3}$$

Figure A1 shows the strength of the first four sidelobes of $f(u)$ vs b_1/b_0. The minimum peak sidelobe level occurs when $b_1/b_0 = 0.852$ which, substituted into Eq. (A1) is

$$A(x) = 0.54 + 0.46 \cos(\pi x/a) \tag{A4}$$

which is the Hamming window. To generate this distribution with a lens, we excite three feed elements with currents of 0.426, 0.1, and 0.426.

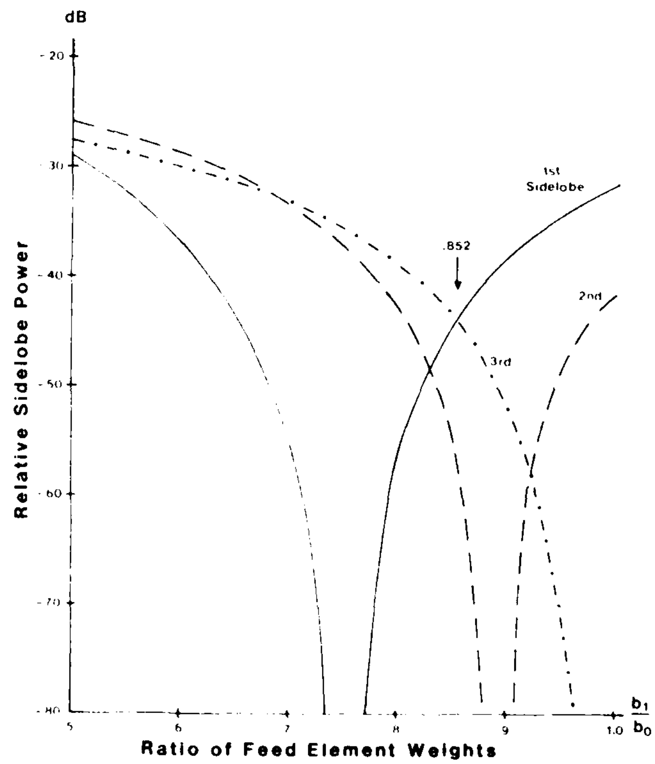

Figure A1. Sidelobe Levels vs Beam Port Weights, Line Source

A2. THREE-DIMENSIONAL LENS, CIRCULAR APERTURE

In a manner analogous to Eq. (A1), Ruze[A1] expresses the distribution F(r) in a circular aperture of radius a as:

$$A(r) = \sum_n b_n J_0(\gamma_n r) \tag{A5}$$

If the beams formed by each term of the summation are to be orthogonal, then γ_n's are the roots $J_1(\gamma_n) = 0$, or $\gamma_0 = 0$, $\gamma_1 = 3.8317$, $\gamma_2 = 7.0156$, and so on. The far field pattern is then:

$$f(u) = 2\pi a^2 \sum_n b_n J_0(\gamma_n) \frac{u J_1(u)}{u^2 - \gamma_n^2} . \tag{A6}$$

Again, if we allow only two terms, then:

$$\frac{f(u)}{2\pi a^2} = \frac{J_1(u)}{u} - 0.4028\, b_1 \frac{u J_1(u)}{u^2 - 3.8317^2} \tag{A7}$$

where $b_0 = 1$. Figure A2 shows that the lowest peak sidelobe level occurs when $b_1/b_0 = 1.925$. To generate a good approximation to this distribution we use a seven-element feed with six elements forming a hexagon around the center elements. The center port is excited with current $b_0 = 1$ and the outer elements with $b_1/6$, or 0.3208 (-9.874 dB).

A1. Ruze, J. (1964) Circular aperture synthesis, <u>IEEE Trans. Antennas Propag.</u> pp. 691-694.

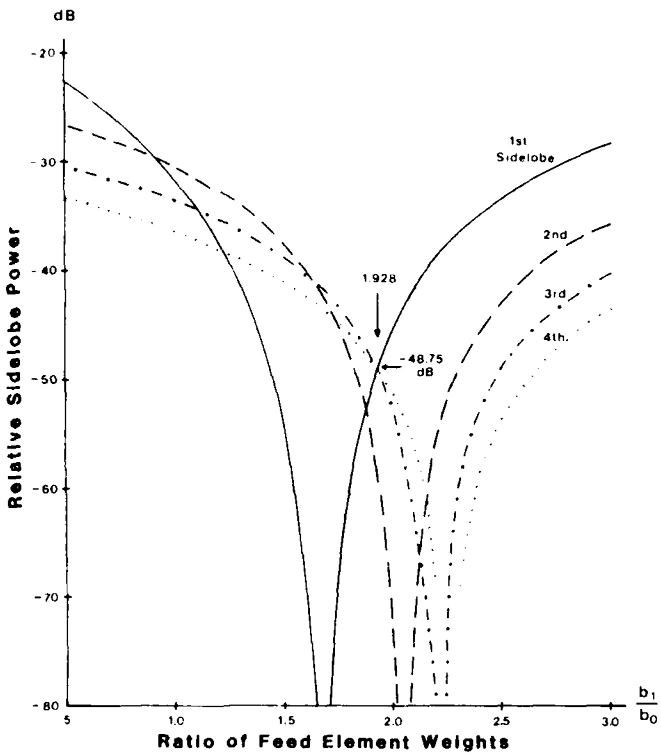

Figure A2. Sidelobe Levels vs Beam Port Weights, Circular Aperture

MISSION
of
Rome Air Development Center

RADC plans and executes research, development, test and selected acquisition programs in support of Command, Control Communications and Intelligence (C^3I) activities. Technical and engineering support within areas of technical competence is provided to ESD Program Offices (POs) and other ESD elements. The principal technical mission areas are communications, electromagnetic guidance and control, surveillance of ground and aerospace objects, intelligence data collection and handling, information system technology, solid state sciences, electromagnetics and electronic reliability, maintainability and compatibility.

Printed by
United States Air Force
Hanscom AFB, Mass. 01731

END

FILMED

6-85

DTIC